
This is an electronic reprint of the original article.
This reprint may differ from the original in pagination and typographic detail.

Turunen, Teemu T.; Koskelainen, Ari
Transretinal ERG in studying mouse rod phototransduction

Published in:
Investigative Ophthalmology and Visual Science

DOI:
[10.1167/iavs.17-22248](https://doi.org/10.1167/iavs.17-22248)

Published: 01/12/2017

Document Version
Publisher's PDF, also known as Version of record

Published under the following license:
CC BY-NC-ND

Please cite the original version:
Turunen, T. T., & Koskelainen, A. (2017). Transretinal ERG in studying mouse rod phototransduction: Comparison with local ERG across the rod outer segments. *Investigative Ophthalmology and Visual Science*, 58(14), 6133-6145. <https://doi.org/10.1167/iavs.17-22248>

This material is protected by copyright and other intellectual property rights, and duplication or sale of all or part of any of the repository collections is not permitted, except that material may be duplicated by you for your research use or educational purposes in electronic or print form. You must obtain permission for any other use. Electronic or print copies may not be offered, whether for sale or otherwise to anyone who is not an authorised user.

Transretinal ERG in Studying Mouse Rod Phototransduction: Comparison With Local ERG Across the Rod Outer Segments

Teemu T. Turunen and Ari Koskelainen

Department of Neuroscience and Biomedical Engineering, Aalto University School of Science, Espoo, Finland

Correspondence: Ari Koskelainen, Department of Neuroscience and Biomedical Engineering, Aalto University School of Science, P.O. Box 12200, FI-00076 Aalto, Finland; ari.koskelainen@aalto.fi.

Submitted: May 18, 2017
Accepted: October 29, 2017

Citation: Turunen TT, Koskelainen A. Transretinal ERG in studying mouse rod phototransduction: comparison with local ERG across the rod outer segments. *Invest Ophthalmol Vis Sci.* 2017;58:6133–6145. DOI:10.1167/iov.17-22248

PURPOSE. Electroretinography (ERG) is the gold standard in clinical examinations of retinal function. Corneal ERG is widely used for diagnostics, but ERG components from the inner retina complicate quantitative investigations of the phototransduction cascade. Transretinal ERG (TERG) recorded *ex vivo* enables pharmacologic isolation of signals generated by photoreceptor cells, establishing an appealing electrophysiologic method for diverse studies of phototransduction. Pharmacologically isolated TERG, however, contains components arising in the photoreceptor inner segments. Here, we compared simultaneously recorded TERG and local ERG across the outer segment layer (LERG-OS) to determine how consistently TERG reflects changes in the rod outer segment current signaling.

METHODS. Recordings were made from dark-adapted, isolated C57BL/6J mouse retinas superfused with HEPES or bicarbonate buffered solution containing 2-mM aspartate or 20- μ M DL-2-amino-4-phosphonobutyric acid to block synaptic transmission, and 50- μ M BaCl₂ to block the Müller cell component. TERG responses were recorded with macroelectrodes on both sides of the retina while responses across different retinal layers were recorded with microelectrodes.

RESULTS. The time-to-peak and the dominant time constant values were slightly smaller and the half-saturating stimulus was somewhat stronger in TERG compared with LERG-OS. No differences in light adaptation data were observed between the methods. LERG responses recorded across the whole photoreceptor layer were similar to those by TERG.

CONCLUSIONS. TERG photoreceptor responses correspond well with the LERG-OS responses. The main differences are the nose component and slightly faster response kinetics observed by TERG. We conclude that TERG can be used for reliable quantitative investigation of phototransduction.

Keywords: phototransduction, retinal pharmacology, rods, cones, light adaptation

Full-field electroretinography (ERG) remains the gold standard in investigating retinal function.¹ Moreover, recording corneal ERG from anesthetized animals is the most widely applied electrophysiologic method for assessing retinal function in wild-type as well as in eye-disease model animals. Recent advances in genetic engineering have resulted in an expanding number of animal models for various eye diseases. Many of these retinal disorders, including retinitis pigmentosa,^{2,3} congenital stationary night blindness,^{4,5} certain forms of achromatopsia,^{6,7} and cone-rod dystrophies⁸ derive from dysfunctions in photoreceptor cells. However, the photoreceptor component in corneal ERG is mostly masked by the superimposed signals from other retinal cells crucially limiting the information available from photoreceptors. Additionally, in the corneal ERG studies of preclinical drug efficiency and drug safety testing, quantitative pharmacologic manipulation of the retinal cells is challenging, because the drug concentrations in the target cells are hard to control *in vivo*. Thus, electrophysiologic approaches allowing precise control of drug concentration as well as separation of the signal components arising from different cell types would greatly benefit preclinical studies of the molecular mechanisms of drug actions.

Transretinal ERG (TERG) provides a straightforward *ex vivo* technique for quantitative electrophysiologic examination of retinal function in an isolated retina.^{9–11} TERG has an excellent signal-to-noise ratio enabling response detection on a level clearly below single absorbed photon per cell.^{12,13} In TERG experiments, retinal cells preserve their natural connections enabling retinal signaling to remain stable for long periods (up to 1 day). Above all, TERG allows pharmacologic manipulation of cells and dissection of signal components from different cell layers by changing the content of the solution superfusing the retina.¹⁴

Earlier studies have shown that transretinally recorded ERG photoresponses closely correspond to corneal ERG responses.^{13,15,16} In this paper, we investigate the possible limitations of TERG in studying phototransduction by examining the correspondence between pharmacologically isolated photoreceptor TERG responses and the light-induced changes in the photoreceptor outer segment current. According to the present understanding, pharmacologically isolated photoreceptor TERG signal mainly reflects changes in the rod outer segment current, but the signal components from the photoreceptor



inner segments are assumed to modify the photoresponses.^{12,14,17-19}

Direct registration of the circulating current from a single photoreceptor, feasible by suction pipette recordings,²⁰ is the standard method for studying phototransduction. However, suction pipette recordings are technically demanding and do not allow straightforward manipulation of the solution surrounding the cell inside the pipette. Another method for monitoring the changes in the circulating current is to record the potential difference (i.e., local ERG) across the photoreceptor outer segment layer with microelectrodes (LERG-OS). The cyclic guanosine monophosphate-gated channels, through which the circulating current enters the photoreceptor cells, are the only functional ion channels present in the outer segments, and therefore the voltage across outer segment layer is linearly related to the circulating current.^{17,21} Thus, placing ERG electrodes at the distal and proximal ends of the outer segment layer allows recordings that directly reproduce the changes in the outer segment current controlled by phototransduction. This study compares simultaneously recorded TERG and LERG-OS photoresponses. We show that blocking synaptic transmission with 20- μ M DL-2-amino-4-phosphonobutyric acid or 2-mM sodium aspartate combined with 50- μ M BaCl₂ to abolish the Müller cell signaling do not compromise phototransduction. In addition, we demonstrate that the LERG-OS signals emerge purely from rods and that the cone contribution to ERG arises predominantly in the photoreceptor inner segment layer. Furthermore, our investigation reveals that, besides the fast “nose” component, an additional component originating in the rod inner segment layer can shape the TERG responses. Nevertheless, the similarity of waveforms and kinetics of photoresponses by the two methods with all the common experimental paradigms indicates that TERG can be adopted not only for qualitative examinations of retinal function but also for quantitative studies of phototransduction.

METHODS

Ethical Approval

The use and handling of the animals were in accordance with the ARVO Statement for the Use of Animals in Ophthalmic and Vision Research, with Finnish Act on Animal Experimentation 2006, and guidelines of the Animal Experiment Board in Finland.

Animals and Preparation

Wild-type mice (C57BL/6J) were dark-adapted overnight and killed by CO₂ inhalation and cervical dislocation. The eyes were enucleated and a small incision was made along the equator of the eyes. The eyes were bisected by enlarging the incision with micro scissors and the isolated eyecup was placed into cooled nutrition solution (composition described in the below Perfusion and Temperature section). One eyecup was stored at 7°C in nutrition solution inside a light tight container to be used later during the same day. The retina was removed from the eyecup under a microscope and the whole retina was placed in a recording chamber inside a Faraday cage. All procedures were completed under dim red light.

Recording Chamber

Figure 1 shows the structure of the recording chamber that is open from above. An isolated retina was placed photoreceptor side upward on a filter paper, glued on a dome in the back piece of the recording chamber, and the retina was held in

place by gently clamping the rim of the retina between two accurately fitting polycarbonate pieces. The electrical connection between the distal and proximal sides of the retina was minimized with a rubber seal covered with vacuum grease. The retinas were illuminated with infra-red (IR) light from 810-nm light emitting diode (SHPL-810-260; Roithner Lasertechnik GmbH, Vienna, Austria) filtered with 850 nm long pass filter (SCHOTT Scandinavia, Lyngby, Denmark) and viewed with an IR-sensitive video camera (KPC-310BH; KT&C, Seoul, Korea) through a glass window underneath the retina. During the experiments, the recording chamber was filled with nutrition solution. The light stimuli were guided to the retina through a glass window at the end of the chamber allowing light stimulation parallel with the longitudinal axis of photoreceptors.

Perfusion and Temperature

A constant laminar flow of the nutrition solution (*ca.* 3 mL/min) perfused the photoreceptor side of the retina. We used two different nutrition solutions: composition of HEPES buffered solution was (mM): Na⁺, 133.4; K⁺, 3.3; Mg²⁺, 2.0; Ca²⁺, 1.0; Cl⁻, 143.2; glucose, 10.0; EDTA, 0.01; HEPES, 12.0, adjusted to pH 7.5 with 5.8 mM NaOH. Composition of the bicarbonate buffered solution was (mM) Na⁺, 124.3; K⁺, 3.3; Mg²⁺, 2.0; Ca²⁺, 1.0; Cl⁻, 133.6; glucose, 10.0; EDTA, 0.01; HEPES, 10.0; NaOH, 4.8; NaHCO₃, 20. Both solutions contained 0.72-mg/mL Leibovitz culture medium L-15 to improve the viability of the retina. Synaptic transmission to bipolar cells was blocked with 2-mM sodium aspartate in HEPES buffered solution and with 20- μ M DL-2-Amino-4-phosphonobutyric acid (APB) in bicarbonate buffered solution.¹⁰ The glial component arising from Müller cells was abolished by adding 50- μ M BaCl₂ to solutions.^{10,22} HEPES, present in both solutions, also blocks the pH-sensitive feedback form horizontal cell to cone photoreceptors although its main purpose in our study was pH buffering.^{23,24} All chemicals were purchased from Sigma-Aldrich (Espoo, Finland). The perfusion was connected to the signal ground with a 4.7- μ F capacitor to filter high-frequency noise.

The recording chamber was placed on top of a heat exchanger connected to a water circulating heating bath (LTD6G; Grant Instruments Ltd, Shepreth, Royston, UK). All recordings were conducted at a temperature of 37 \pm 1°C. The temperature was measured in the immediate vicinity of the surface of the retina with a calibrated thermistor (30K6A309I; BetaTHERM; Measurement Specialties, Inc., Hampton, VA, USA) at the beginning and at the end of each experiment.

Recordings

Transretinal ERG. There were Ag/AgCl pellet macroelectrodes (EP2; World Precision Instruments Ltd [WPI], Hitchin, UK) used to record TERG. One of the electrodes was inserted into an electrode space connected to the proximal side of the retina through a ϕ 0.8-mm hole, covered with a filter paper. This set the active recording area to 0.5 mm². The other electrode was connected to the open chamber through a small channel. Both electrode spaces were filled with a chloride solution containing 115-mM Na⁺, 122.3-mM Cl⁻, 3.3-mM K⁺, and 2.0-mM Mg²⁺.

Local ERG. Local ERG was recorded with two microelectrodes. The Ag/AgCl pellet electrodes were connected to micropipettes through a custom made connector. Pipettes were pulled from glass capillaries (TW100-6; WPI) with a micropipette puller (Model P-97; Sutter Instrument Co.,

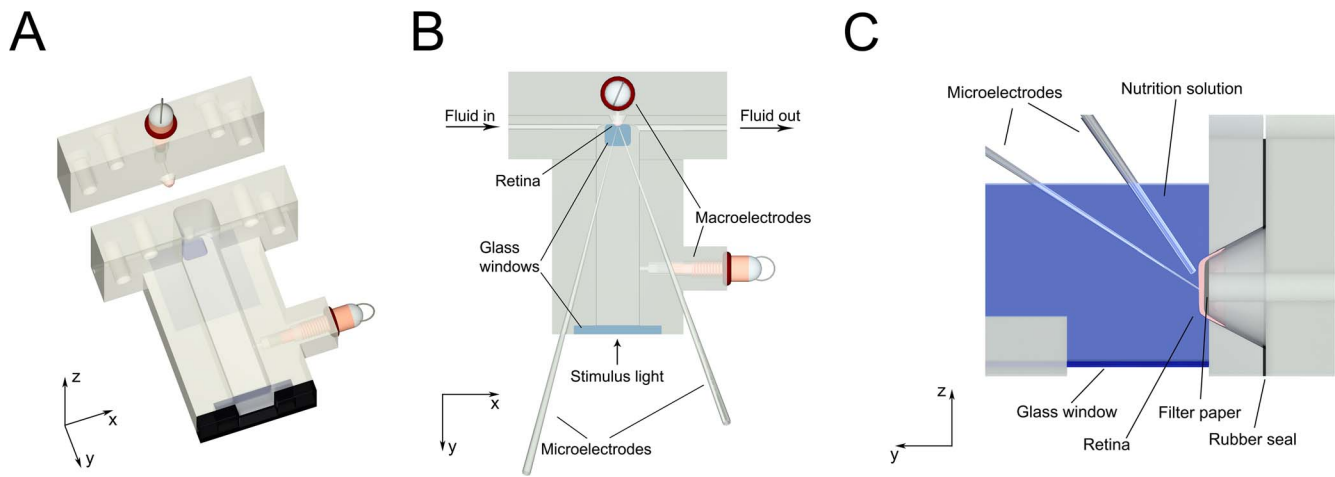


FIGURE 1. The design of the recording chamber used to record simultaneous TERG and LERG responses. **(A)** The two parts comprising the recording chamber. **(B)** The recording geometry. The open pool in the recording chamber was filled with nutrition solution and the retina was viewed through the bottom glass window. TERG was recorded with macroelectrodes placed at the distal and proximal side of the retina. LERG was recorded across the desired retinal layer with microelectrodes. **(C)** Positioning of the microelectrodes. Before and after each recording session, the temperature of the retina was measured with a thermistor brought to the surface of the retina with a micromanipulator.

Novato, CA, USA) and filled with the chloride solution described above. The tip diameters were 2 to 5 μm for the recording electrode and *ca.* 30 μm for the reference electrode. The recording electrode position was controlled with a hydraulic micromanipulator (MC-35A, 0.2- μm resolution; Narishige International Ltd., London, UK) and the reference electrode was moved with an electronic micromanipulator (MR 471843; Carl Zeiss AG, Oberkochen, Germany). In local ERG across the photoreceptor outer segment layer (LERG-OS) the recording electrode was advanced to a depth of *ca.* 25 μm from the photoreceptor tips and in LERG across the whole photoreceptor layer (LERG-PR) to a depth of *ca.* 100 μm . The recording electrode was placed to the central region of the retina and it was advanced at an angle of 30° to the long axis of photoreceptors to minimize possible damages to the cells and to reduce blockage of light by the glass pipette in the recording area. The reference electrode was located in the immediate proximity of the surface of the retina (Fig 1C). The glass pipettes had no discernible effects on TERG responses.

Light Stimulation

Flashes (1 ms) or steps of light were produced with two LED light sources (Philips Luxeon Revel LXML-PM01-0100, $\lambda_{\text{max}} = 532$ nm; Lumileds, Amsterdam, Netherlands) and the light was guided to the retina with an optical system consisting of lenses and a dual branch mixing light guide. The stimulus light intensity was controlled with voltage-to-current converters driving the LEDs and with neutral density filters. The stimuli illuminated the flat-mounted part of the retina uniformly as verified with a camera-based beam profiler (Model SP503U; Spiricon Laser Beam Diagnostics, Ophir-Spiricon Inc., Logan, UT, USA). The absolute light intensity incident on retina was measured with a calibrated photodiode (FDS100-cal; Thorlabs GmbH, Newton, NJ, USA). The number of rhodopsin photoisomerizations in rods ($R^*\text{rod}^{-1}$ or $R^*\text{rod}^{-1}\text{s}^{-1}$) were calculated based on the rod outer segments dimensions ($\phi = 1.4$ μm , $l = 24$ μm), the LED emission spectrum, the photodiode absorption spectrum, and the visual pigment template by Govardovskii et al.²⁵ as described in Ref. 26, leading to a stimulus-specific rod collecting area of $a_c = 0.46$ μm^2 .

Data Acquisition

Data acquisition and the control of LEDs were carried out with a data acquisition card (PCIe-6351; National Instruments, Austin, TX, USA) and a custom made LabVIEW software. The recorded signals were amplified 1000-fold and sampled at 1000 Hz with a voltage resolution of 15 nV in the two recording channels (TERG and LERG). The signals were low-pass filtered with $f_c = 500$ Hz (8-pole Bessel filter) and later digitally filtered with $f_c = 100$ Hz.

Analysis

The operation range of rods was determined from stimulus strength-response amplitude curve, where the peak amplitudes of the responses normalized by the saturation amplitude ($r(\Phi) = R(\Phi)/R_{\text{sat}}$) are plotted against stimulus strengths. A linear combination of exponential and Michaelis saturation functions was fitted to the data to define the half-saturating flash strength $\Phi_{1/2}$

$$r(\Phi) = \alpha \left(1 - 2^{-\frac{\Phi}{\Phi_{1/2}}} \right) + (1 - \alpha) \left(\frac{\Phi}{\Phi + \Phi_{1/2}} \right), \quad (1)$$

where Φ is the flash strength in photoisomerisations per rod.¹⁰ This arbitrary function describes the two characteristics of photoresponse amplitude behavior—linear phase at low-flash strengths and saturation of response amplitudes at high-flash strengths.

The Lamb and Pugh phototransduction model (Eq. 2) was fitted to the early phase of normalized, sub-saturated responses to study the kinetics of the photoresponse leading edge. In Equation 2 $r(t)$ is the normalized waveform of the response, t_d is the sum delay in phototransduction and in the measurement device, and A is the activation coefficient describing the amplification in the phototransduction cascade.²⁷

$$r(t) = 1 - e^{-1/2 A \Phi (t - t_d)^2} \quad (2)$$

Contrary to other analysis, responses were low-pass filtered with $f_c = 500$ Hz. For mouse rods, the lifetime of activated rhodopsin is estimated to be as short as 40 ms.²⁸ To minimize the effect of deactivation mechanisms to activation constant determination, the model was fitted from zero time point

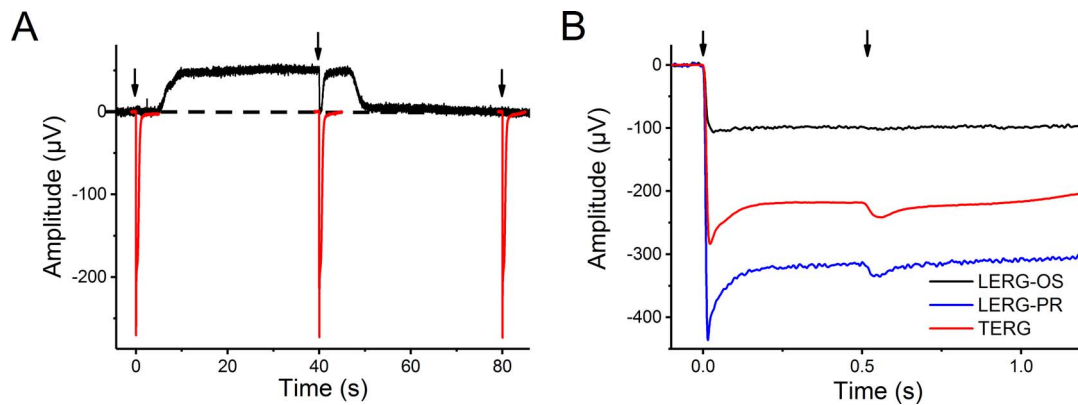


FIGURE 2. (A) Comparison of LERG-OS dark voltage and the voltage suppressible by light. The recording microelectrode was passed from the tip level of the photoreceptors to the depth of the rod cilium ($\sim 25 \mu\text{m}$) and returned back. The retina was stimulated with saturating light flashes ($1580 \text{ R}^*\text{rod}^{-1}$, indicated by arrows). The voltage was recorded continuously by LERG (black trace) and for short stretches by TERG covering the responses (red traces). (B) Double-flash recordings revealing cone and nose components. Rod saturating flashes ($6800 \text{ R}^*\text{rod}^{-1}$) were presented at time points 0 seconds and 500 ms. The cone component (second flash) was absent in LERG-OS recordings but existed in LERG-PR and TERG recordings. HEPES buffered solution.

(indicating the time of the flash) to the time point where the response reached 50% of its peak amplitude or to 40 ms, if the 50% level was reached later. The responses were normalized to the saturation amplitude in LERG-OS recordings and to the plateau level after the fast transient peak in TERG and LERG-PR recordings. In the fittings, t_d varied freely within interval 4 to 7 ms, including a constant 1-ms delay from the filtering.

Sensitivity regulation in background light was studied by fitting the Weber-Fechner function (Eq. 3). In Equation 3 $S_A(I)$ is the absolute rod sensitivity to dim flashes defined as the dim flash amplitude divided by the stimulus strength ($\mu\text{V}/\text{R}^*\text{rod}^{-1}$), $S_{A,\text{dark}}$ is absolute rod sensitivity in darkness, I is the background light intensity ($\text{R}^*\text{rod}^{-1}\text{s}^{-1}$), and $I_{1/2}$ corresponds to the background intensity that halves the sensitivity.

$$\frac{S_A(I)}{S_{A,\text{dark}}} = \frac{I_{1/2}}{I_{1/2} + I}, \quad (3)$$

RESULTS

Changes in Rod Outer Segment Current Can Be Monitored With Local ERG Across Outer Segments

Maximal Photovoltage is Equal to the Dark Voltage Shift Caused by The Electrode Protrusion Into the Outer Segment Layer. In their classical work, Hagins et al.²¹ concluded that in dark-adapted rat rods the light-induced extracellular potential change, the photovoltage, is a result from changes in a single process, the circulating dark current, which has its sinks in the outer segments and sources in the inner segments of rods. Their deduction was elaborated by Arden,¹⁷ who showed that an additional component originating in the rod inner segments adds to the photovoltage. Still, across the rod outer segment region, the maximal photovoltage equals to the dark voltage, induced by the circulating dark current, but with opposite polarity. These results suggest that photovoltage recordings across the outer segment layer faithfully reflect the changes in the circulating current. However, contrary to the results of Arden,¹⁷ the recordings of Green and Kapousta-Bruneau¹⁴ show a photovoltage outweighing the dark voltage in every retinal depth. The obvious difference between the experiments by Hagins et al.²¹ and Arden¹⁷ compared with those by Green and Kapousta-

Bruneau¹⁴ was in their recording geometries. Hagins et al.²¹ and Arden¹⁷ had blocked the electrical connection between the two sides of the retina, while Green and Kapousta-Bruneau¹⁴ had immersed the retina attached on a mesh in the perfusing solution.

To address whether the changes in the rod outer segment current are directly reflected to the local ERG signal across the LERG-OS in our recording geometry, we tested the relation between the dark voltage and the light-induced voltage change in conditions where synaptic transmission from photoreceptor cells was blocked. Figure 2A shows that when the recording electrode started to advance into the retina from the level of the tips of rod outer segments (which corresponds to the level of the tip of the reference electrode), the recorded voltage (black trace) began to increase. When the recording electrode had moved to the level of photoreceptor cilium ($25 \mu\text{m}$), a rod-saturating flash ($1580 \text{ R}^*\text{rod}^{-1}$) was given (at time point 40 seconds in Fig. 2A). The amplitude of the rod saturating response equals to the voltage shift induced by the penetration of the pipette into the outer segment layer, indicating that the circulating outer segment current in the extracellular space of photoreceptors causes the voltage shift. This dark voltage shift was fully reversible when the recording electrode was drawn back to the surface of the retina (at times after 45 seconds in Fig. 2A), where flashes of light caused no response. Simultaneously recorded TERG responses (red traces) did not change during this procedure. Hence, when recorded across the outer segment layer, LERG photoresponses seem to purely reproduce the changes in the outer segment current in the mouse retina.

In most experiments, the saturated LERG-OS response amplitude accurately corresponded to the dark voltage. However, sometimes a reverted miniature version of TERG response appeared to be coupled to the LERG signal, resembling the phenomenon illustrated by Green and Kapousta-Bruneau¹⁴ (data not shown). This coupling of TERG to LERG-OS signal appeared to be associated with loose attachment of the retina to the recording chamber, likely letting part of the rod circulating current to “leak” around the edge of the retina. We conclude that the supplementary ERG component observed by Green and Kapousta-Bruneau¹⁴ is most probably due to the shunt currents around the edge of the retina and a careful isolation of electrical connection between retinal sides disposes the phenomenon.

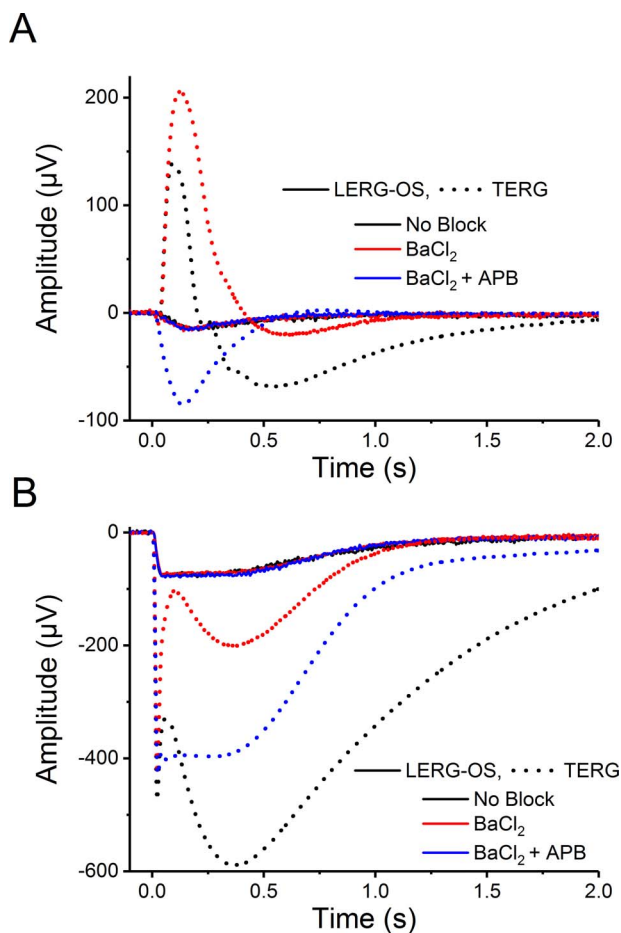


FIGURE 3. Simultaneously recorded TERG and LERG-OS responses to (A) dim flash ($13 \text{ R}^*\text{rod}^{-1}$) and (B) saturating ($1590 \text{ R}^*\text{rod}^{-1}$) stimuli in bicarbonate buffered solution. TERG was recorded without any blockers (black traces) in the presence of $50\text{-}\mu\text{M}$ BaCl_2 (red traces) and in presence of both $50\text{-}\mu\text{M}$ BaCl_2 and $20\text{-}\mu\text{M}$ APB (blue traces).

Cone Contribution is Not Visible in Mouse LERG-OS.

The photoreceptor ERG signal is a superposition of extracellular potential changes caused by both rods and cones. In the mouse retina the cone density is less than 1/30 of the rod density²⁹ and the light sensitivity of rods exceeds that of cones by 1000-fold.¹⁵ Therefore, in dark-adapted retinas the ERG signal is expected to originate mainly from rods. Cone signals can be extracted from TERG by applying a strong cone stimulating flash briefly after a rod saturating flash.²⁶ To investigate how much cones can contribute to LERG-OS, we applied the double-flash approach with simultaneous TERG and LERG-OS recording. Figure 2B represents responses recorded by TERG (red) and LERG-OS (black) with synaptic transmission blocked in order to remove the contribution from second- and higher-order neurons in HEPES buffered solution. In the red TERG trace, a transient “nose” component is apparent after the first flash given at 0 seconds and a cone response after the second, similar flash given at 0.5 seconds. Neither of those is visible in the LERG-OS response. When the LERG recording electrode was advanced deeper, approximately to the level of photoreceptor synapses, the shape of the LERG signal recorded across the photoreceptor layer (LERG-PR, blue) closely corresponded to the TERG signal (the larger photoreponse amplitude by LERG-PR compared with TERG reflects our observation that the maximal response amplitude varied locally in the retina

and that we tried to maximize the LERG response amplitudes with the choice of the point of recording). This indicates that cones do not contribute significantly to the LERG-OS signal and that the cone component present in TERG is generated mainly at the level of photoreceptor inner segments. These data suggest that LERG-OS reflects changes purely in the rod outer segment current and that it can be used as a reference when comparing the properties of TERG with rod outer segment current signals.

Pharmacologic Isolation of the Photoreceptor Component in TERG Does Not Compromise Rod Phototransduction.

Figure 3 shows simultaneously recorded dim ($13 \text{ R}^*\text{rod}^{-1}$, Fig. 3A) and rod-saturating ($1590 \text{ R}^*\text{rod}^{-1}$, Fig. 3B) flash responses across the whole retina (TERG, dashed lines) and across the outer segment layer (LERG-OS, solid lines) in the absence of pharmacologic blockers (black lines), in the presence of $50\text{-}\mu\text{M}$ BaCl_2 (red lines), and in the presence of $50\text{-}\mu\text{M}$ BaCl_2 + $20\text{-}\mu\text{M}$ APB (blue lines) in bicarbonate buffered solution. The saturated LERG-OS responses display clear plateau and the dim flash responses follow the shape of skewed bell curve in all solutions, resembling the waveforms of responses obtained with suction pipette recording from single mouse rods.^{28,30} The saturated TERG response without blockers (black dashed trace in Fig. 3B) shows an a-wave with an amplitude several-fold larger than the LERG-OS response amplitude but the dim flash response (black dashed trace in Fig. 3A) reveals only a hint of a-wave. In both dim and saturated TERG responses the a-wave is followed by a b-wave and a slower glial component from Müller cells, both overlapping with most of the LERG-OS response. In this experiment, b-wave appeared rather small compared with the a-wave amplitudes. Addition of BaCl_2 removes a slow component in the TERG signals, consistent with the removal of the glial component (red dashed trace), without significant effects on the a- or b-wave early onset. Introduction of APB for removing synaptic transmission unveils the photoreceptor component of TERG (blue traces in Figs. 3A, 3B). In solution with APB alone, the slow glial component would dominate the TERG signal after the a-wave and lead to delayed response deactivation and larger signal amplitudes (see Fig. 2D from Ref. 31 for action of APB on TERG photoresponses). The waveforms of the pharmacologically isolated TERG photoreceptor signals appear to resemble the LERG-OS signals well, with the exception of the fast nose component in the saturated TERG response (see also Fig. 2B). The blockers seemed to have little or no effect on LERG-OS responses.

To investigate the possible effects of the pharmacological blocking agents on rod phototransduction more closely, we compared the LERG-OS photoresponses without and in the presence of the blockers in HEPES buffered solution. Figure 4A presents the effect of the synaptic blockers APB ($20 \mu\text{M}$, red traces) and aspartate (2 mM , blue traces) on LERG-OS dim and saturating flash photoresponses. Reference responses were recorded before and after the use of blockers (before, black traces; after, gray). Practically no effect could be seen in the LERG-OS responses. BaCl_2 ($50 \mu\text{M}$, green traces; before black; after gray), used for blocking Müller cell potassium currents, caused a minor but irreversible decrease in the saturated response amplitude ($<10\%$) and a slight delay in the response shut-off (see Fig. 4B). No effect could be observed on dim flash responses. We conclude that these blockers can be safely used in these concentrations without compromising rod phototransduction.

“Nose” Component Originates in the Inner Segment Region of Photoreceptors. The most notable difference between pharmacologically isolated photoreceptor TERG and LERG-OS responses is the fast transient “nose” component present in TERG but not in LERG-OS in the early phase of

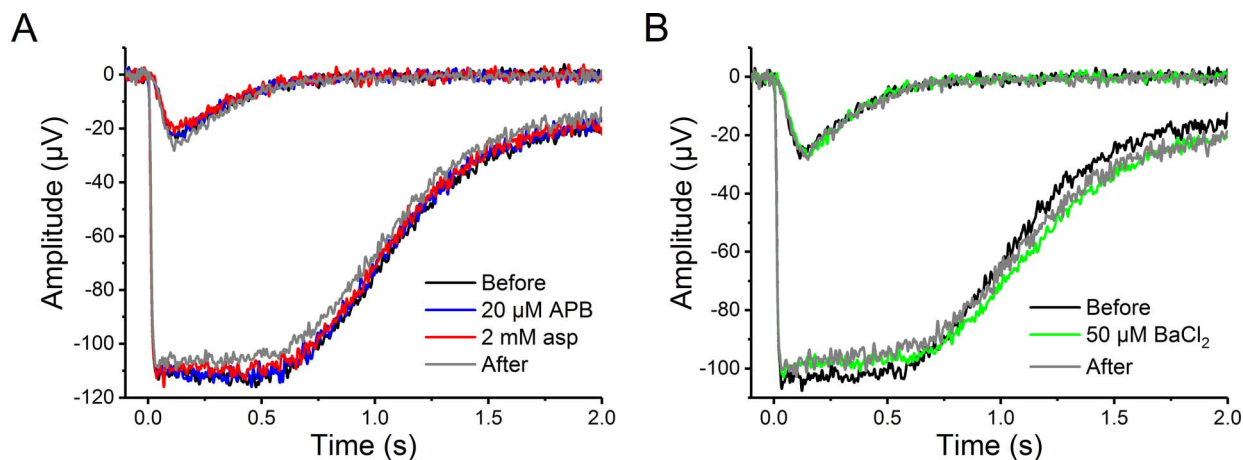


FIGURE 4. The effect of synaptic blockers on dim ($6.8 R^*rod^{-1}$) and saturating flash ($1700 R^*rod^{-1}$) responses in HEPES buffered solution. Reference responses were recorded before the introduction (*black*) and after the washout (*gray*) of blockers. (A) LERG-OS responses recorded with 20- μ M APB (*blue*) and 2-mM aspartate (*red*). (B) LERG-OS responses recorded with 50- μ M $BaCl_2$.

strong flash responses. Figure 5A demonstrates the progression of the saturated LERG response to the same stimulus ($1580 R^*rod^{-1}$) when the recording electrode is advanced from outside of the retina ($-40 \mu\text{m}$) to the approximate level of photoreceptor synapses ($100 \mu\text{m}$). The reference electrode is kept at the distal surface of the retina for the whole measurement. The saturated responses are flat when the electrode tip is at the depths of 10 to $30 \mu\text{m}$. This can be seen more easily in Figure 5B where the signal amplitudes are scaled to coincide at the moment the photoresponses begin to recover (here at 0.45 seconds). With this scaling, the saturated responses recover along a common trajectory independent of the depth of the recording electrode tip. The behavior was similar in both HEPES and bicarbonate buffered solutions. The first signs of the “nose” starts to emerge as the recording electrode passes the outer segment layer, at the depth of approximately $30 \mu\text{m}$. When recording LERG across the whole photoreceptor layer (i.e., at depths of 80– $100 \mu\text{m}$) the response waveform, including the nose, corresponds to that recorded by TERG (black dashed trace).

Comparison of Rod Responses to Various Light Stimuli

To compare TERG and LERG-OS responses in more detail, we used several light stimulus paradigms. Activation and recovery phases of photoresponses were investigated by recording response families to 1-ms flash stimuli covering the operational range of dark-adapted rods. Changes in responses caused by light adaptation were examined with (1) step responses over a large dynamic range, (2) flash responses recorded during steady background lights, and (3) the step-flash paradigm⁵² believed to reflect changes in the activated rhodopsin lifetime. We conducted the experiments in HEPES buffered solution (see Methods) resembling the Locke's solution commonly used to nourish rod outer segments inside the glass capillary in suction pipette recordings. Additionally, we replicated the flash response experiments in bicarbonate buffered solution to mimic the conditions outside the pipette in suction pipette recordings. The used solution is separately mentioned in described experiments and in figure captions.

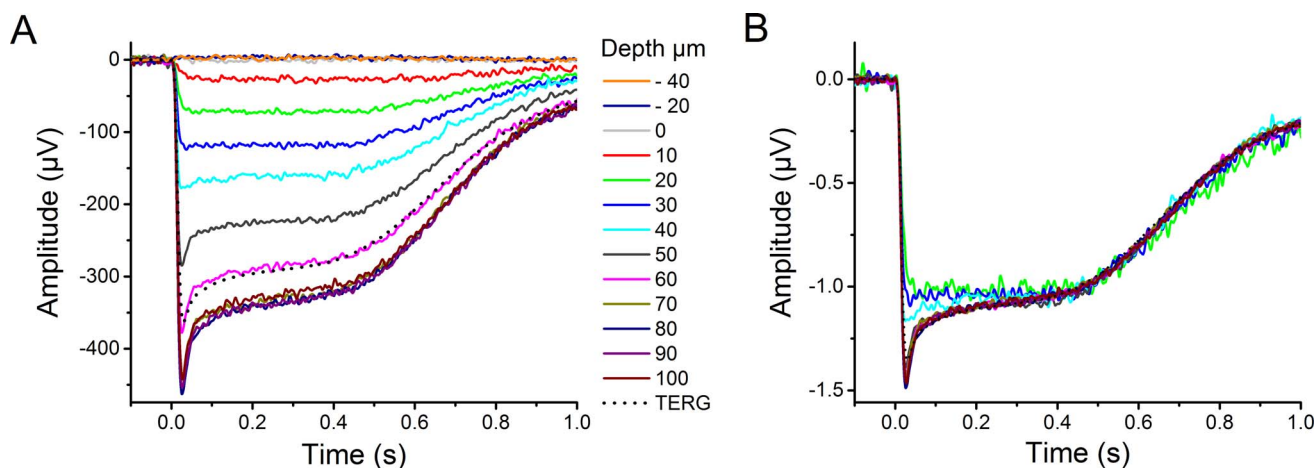


FIGURE 5. (A) LERG responses to saturating light flashes ($1580 R^*rod^{-1}$) at varying retinal depths in HEPES buffered solution. The situation where both the reference and the recording electrodes were on the surface of the retina is indicated by $0 \mu\text{m}$. Simultaneously recorded TERG is shown for comparison (*black dashed trace*). (B) Responses of *panel A* normalized to the level where responses start to return from saturation. Responses recorded at depths of $10 \mu\text{m}$ or below were removed for clarity.

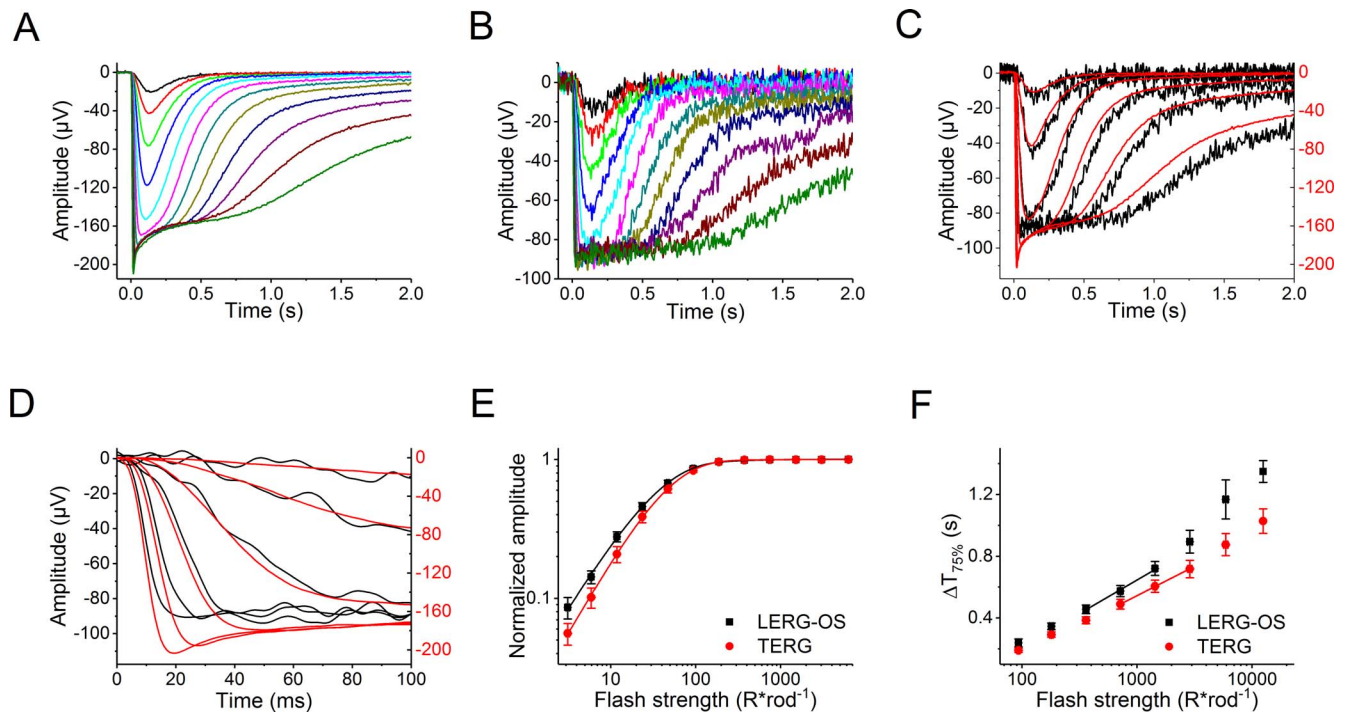


FIGURE 6. Simultaneously recorded flash response families (A) by TERG and (B) by LERG-OS in HEPES buffered solution. (C) TERG (red) and LERG-OS (black) response families scaled to coincide with the saturated response plateau levels. (D) Responses in panel C scaled to show the first 100 ms of the responses. Flash strengths were between 6.3 to 12500 R^*rod^{-1} with 2-fold increments. In (C, D) half of the responses has been omitted for the sake of clarity. Each trace represents a single response without averaging. (E) Normalized stimulus strength-response amplitude curve averaged from eight experiments. The continuous lines show the fittings of Equation 1 to the TERG (red) and LERG-OS (black) data, respectively. (F) Pepperberg plots averaged from seven experiments. The error bars indicate SEMs.

Flash Response Kinetics is Slightly Faster in TERG Compared With LERG-OS. Figures 6A and 6B show rod photoreponse families recorded simultaneously with TERG and with LERG across the outer segment layer in HEPES buffered solution with flash strengths ranging from 6.3 to 12500 R^*rod^{-1} . The TERG and LERG-OS photoreponses show closely corresponding waveforms except for the nose part in the early phase of responses to strong stimuli. However, when the photoreponse families are illustrated in the same panel (Fig. 6C) with the plateau levels scaled to match, the recovery of the TERG responses seems to start earlier than in LERG-OS responses. Figure 6D plots the first 100 ms of the responses presented in Figure 6C. The activation phases of subsaturated TERG and LERG-OS responses coincide well, but with strong flashes, the leading edges of the TERG responses seem to develop slightly faster compared with LERG-OS responses, which could be due to a fast capacitive component described in Ref. 19. Closer investigation by fitting of Lamb and Pugh activation model²⁷ (Equation 2, see Methods for fitting details) to the early phase of the subsaturated responses yielded a minor 16% increase in activation constant determined from TERG compared with LERG-OS in HEPES buffered solutions ($n = 8$ retinas, $P < 0.05$, one-tailed paired t -test).

The rod light sensitivity values appeared greater when determined by LERG-OS than when obtained by TERG. In HEPES buffered solution, the fractional sensitivity (defined as the dim flash response amplitude divided by stimulus strength and saturation amplitude) was 28% smaller and the half-saturating flash strength (Equation 1) was 23% larger by TERG compared with LERG-OS. However, instead of just shifting the stimulus strength-response amplitude curve to higher stimulus strengths, the sensitivity difference partly comes out as a steeper slope of the curve by TERG (Fig. 6E, data averaged over 8 retinas). The

faster photoreponse shut-off kinetics can mostly explain the ostensibly lower light sensitivity by TERG, consistent with the time-to-peak values (t_p) of dim flash responses being 17% smaller by TERG than by LERG-OS. Also, the dominant time constant of saturated photoreponse recovery (τ_D), determined from Pepperberg plots³³ as illustrated in Figure 6F were 16% smaller by TERG. Fitting single exponentials to the late-decay phases of dim flash responses, however, gave similar time constants (τ_{rec}) for both recording geometries, although the variance of τ_{rec} was significantly larger by TERG compared with LERG-OS ($P = 0.001$, one-tailed two-sample F test for variance). The Table summarizes sensitivity and kinetics parameters determined from flash responses by LERG-OS and TERG in both HEPES and bicarbonate buffered solutions.

Additionally, the Table presents the comparison of parameters obtained from simultaneously recorded flash responses by LERG-PR and TERG. No significant differences were observed. The Table also displays a literature review of parameter values derived from suction pipette recordings of mouse rods. The experiments chosen from the literature were conducted in bicarbonate buffered Locke's solution that nourished the cells outside the pipette and with HEPES buffered Locke's solution inside the pipette. The most notable difference between the suction pipette and the ERG techniques is the greater rod sensitivity in suction pipette recordings. The activation coefficients determined by suction pipette recordings varied profoundly in literature (7.9,³⁴ 8.3,³⁵ 20.5,³⁶ and 23³⁷ s^{-2}). Our value was close to the values determined in Refs. 34 and 35 (see Table).

Recovery During Step Responses is Stronger by TERG Compared With LERG-OS. The effect of background light was examined with 9-second light steps with intensities ranging from 2 to 3960 $R^*rod^{-1}s^{-1}$. Figure 7 shows a family

TABLE. Characteristics of Mouse Rod Photoresponses Determined by TERG, LERG-OS, and LERG-PR Recordings in Bicarbonate and HEPES Buffered Solutions

Parameters	Bicarbonate Buffered Solution				HEPES Buffered Solution				Suction Pipette Recordings
	<i>n</i> = 9		<i>n</i> = 6		<i>n</i> = 8		<i>n</i> = 8		
	TERG & LERG-OS		TERG & LERG-PR		TERG & LERG-OS		TERG & LERG-PR		
t_p (ms)	125 ± 9	142 ± 6†	144 ± 20	133 ± 20	148 ± 4	173 ± 8*	138 ± 4	135 ± 8	130–190 (7)
τ_D (ms)	148 ± 7	166 ± 9*	153 ± 9	179 ± 9	168 ± 8	193 ± 9*	166 ± 9	161 ± 7	159–271 (7)
<i>A</i> (s^{-2})	13.4 ± 2.5	10.5 ± 1.2	11.3 ± 1.3	10.7 ± 0.8	8.6 ± 0.8	7.4 ± 0.7*	9.0 ± 1.1	11.1 ± 2.1	7.9–23 (4)
τ_{rec} (ms)	169 ± 16	173 ± 7	176 ± 30	203 ± 36	190 ± 33	181 ± 9	201 ± 15	184 ± 10	201–253 (4)
$\Phi_{1/2}$ (R^*rod^{-1})	55.6 ± 8.8	34.2 ± 3.8†	57.7 ± 9.8	43.1 ± 7.7	36.5 ± 3.6	29.7 ± 3.5*	34.5 ± 3.5	35.4 ± 4.9	13.8–21.7 (5)
S_{Fdark} ($\%/R^*rod^{-1}$)	1.9 ± 0.7	2.3 ± 0.3	1.5 ± 0.3	1.6 ± 0.2	1.8 ± 0.2	2.5 ± 0.2*	2.3 ± 0.3	2.1 ± 0.3	3.6–5.4 (6)
r_{max} (μV)	312 ± 51	105 ± 30†	328 ± 49	378 ± 59	205 ± 21	63 ± 8†	244 ± 41	280 ± 35	12.6–20 pA (7)

TERG experiments were recorded simultaneously with LERG-OS or with LERG-PR. Parameters: t_p , time-to-peak of dim flash response; τ_D , dominant time constant of saturated response recovery obtained from Pepperberg plot; *A*, activation coefficient determined by fitting Lamb and Pugh activation model (Equation 2); τ_{rec} , time constant of single exponential fit to the return phase of dim flash responses; $\Phi_{1/2}$, half-saturating flash strength; S_{Fdark} , dim flash response dark-adapted sensitivity; r_{sat} , saturated response amplitude measured from the response plateau level. Values are reported as mean ± SEM and the number of experiments is given in the header. One-tailed paired student's *t* distribution was used to compare the parameter values obtained with the different recording geometries. The range of published parameter values acquired by suction electrode recordings from mouse rods are presented for comparison. The number of source publications is listed in parenthesis.^{30,34–37,45,46}

* $P < 0.05$.

† $P < 0.01$.

of step responses and a response to a saturating flash given at time $t = 0$ seconds in HEPES buffered solution by simultaneously recorded TERG (panel A) and LERG-OS (panel B). Figure 7C presents the responses from 7A and 7B normalized to the plateau of the saturated flash responses. The response shapes are closely similar between the two recording geometries. However, the step responses by TERG recovered to a level beyond the steady-state level reached by the LERG-OS responses (see also Fig. 9E for an exceptionally large recovery difference). The step light that produced an average steady-state response amplitude of $82 \pm 4\%$ of the saturated flash amplitude recorded by LERG-OS only gave $49 \pm 5\%$ amplitude by TERG. The difference was statistically significant ($n = 6$, $P < 0.001$, one-tailed paired *t*-test).

Light Adaptation Affects TERG and LERG-OS Responses Similarly. Light adaptation of mouse rod phototransduction was investigated by recording dim flash responses during 9-second steps of background light with intensities between 8 and $1980 R^*rod^{-1}s^{-1}$ in HEPES buffered solution. The dim flashes were given at 6 seconds after the light onset. Figures 8A and 8B show the responses from one experiment recorded simultaneously by TERG and LERG-OS, respectively. The absolute rod sensitivity normalized by the sensitivity in darkness (see Methods) is plotted as a function of the increasing background light intensity in Figure 8C, together

with Weber-Fechner function (Equation 3) fitted to the data. The sensitivity halving background light intensity obtained by TERG was $89 \pm 18 R^*rod^{-1}s^{-1}$ and $98 \pm 15 R^*rod^{-1}s^{-1}$ obtained by LERG-OS ($n = 5$). The difference was statistically nonsignificant.

Acceleration of Saturated Response Recovery in Background Light is Analogous by TERG and LERG-OS.

It has previously been shown for amphibian and mouse rods that the time responses spend in saturation reduce in background light due to the decrease in $[Ca^{2+}]_{in}$. It is believed that when calcium unbinds from the calcium sensor protein recoverin, the phosphorylation activity of rhodopsin kinase increases, which reduces the lifetime of activated rhodopsin.^{32,38–40} We tested the background light-induced acceleration of flash response recovery with the step-flash paradigm of Fain et al.,³² assumed to reflect the shortening of activated rhodopsin lifetime, by delivering identical saturating flashes at the same moment the 9-second background light steps turned off. Step-flash experiments were conducted on five retinas in HEPES buffered solution with step-light intensities ranging from 2 to $3960 R^*rod^{-1}s^{-1}$. Figure 9A shows responses from a single step-flash experiment recorded by TERG and Figure 9C shows simultaneously recorded LERG-OS responses. The striking difference between the TERG and LERG-OS step-flash responses is that the saturated TERG flash

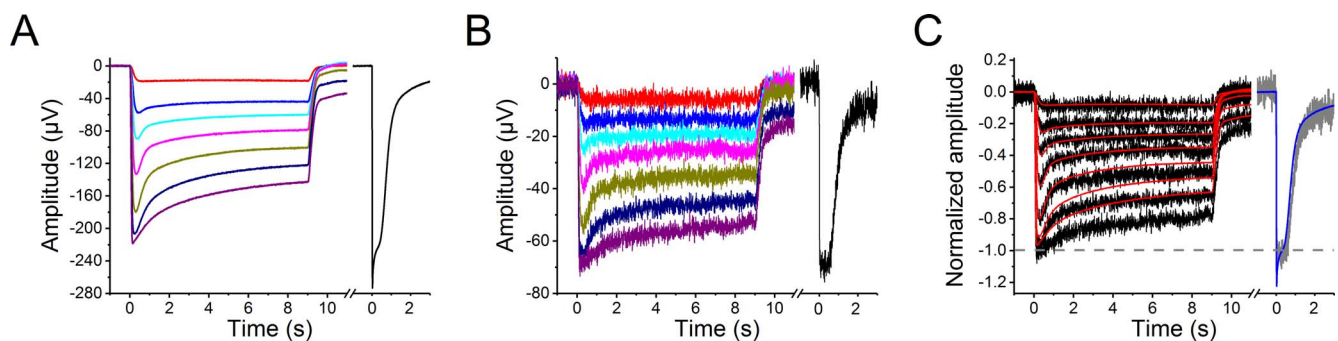


FIGURE 7. Simultaneously recorded responses to 9-second steps of light (31 – $1980 R^*rod^{-1}s^{-1}$) with 2-fold increments and to a saturating flash ($1580 R^*rod^{-1}$) (A) by TERG and (B) by LERG-OS in HEPES buffered solution. (C) TERG (red) and LERG-OS (black) response families are scaled to coincide at the plateau levels of saturating flash responses (LERG-OS, gray; TERG, blue).

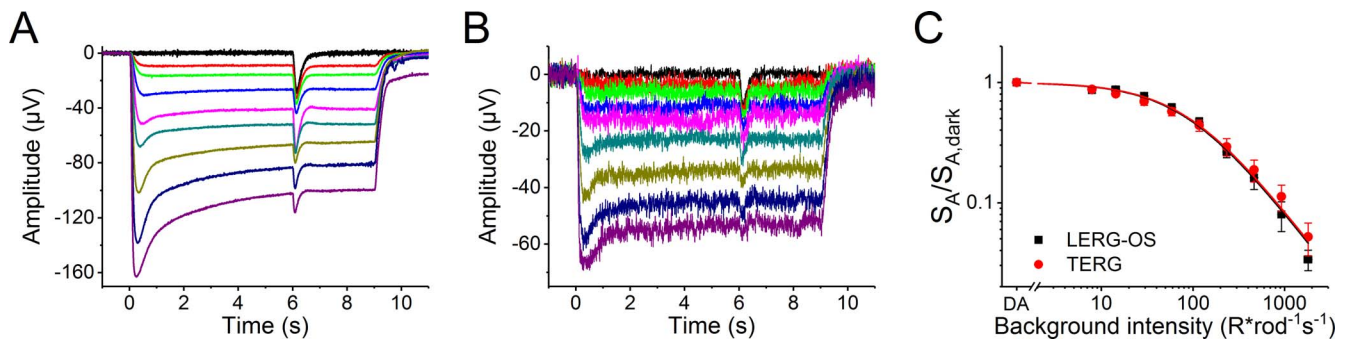


FIGURE 8. Dim flash responses recorded in darkness and during steps of light (A) by TERG and (B) by LERG-OS in HEPES buffered solution. The background light intensities were between 8 to 990 $R^*rod^{-1}s^{-1}$ with 2-fold intensity increments. (C) Dim flash sensitivity plotted against background light intensity in log-log scale from population-averaged data from five experiments. Fitting of Equation 3 to the data gave $I_{1/2}$ of $91.1 \pm 5.1 R^*rod^{-1}s^{-1}$ by TERG (red) and $87.5 \pm 4.8 R^*rod^{-1}s^{-1}$ by LERG-OS (black). Dim flash strengths varied from 3 to 99 R^*rod^{-1} .

responses do not settle to a common level but instead, the response saturation level declines with increasing background light intensity. With the strongest step intensity the flash response saturation level declined by $33 \pm 5\%$ ($n = 5$) compared with that in darkness. Similar behavior of the saturation level appeared in LERG-PR step-flash recordings (data not shown). In LERG-OS, this kind of behavior was absent and the saturated flash responses settled to a common level. There was a strong correlation (correlation coefficient of 0.97, $n = 5$) between the relative decrease in TERG saturated flash-response amplitude at step-light offset and the relative difference in TERG and LERG-OS step response steady-state amplitudes. Figure 9E shows TERG and LERG-OS step-flash responses with step-light intensity 1580 $R^*rod^{-1}s^{-1}$ from a single experiment. The responses are normalized with the plateau levels of saturated flash-response amplitudes in darkness. In addition, Figure 9E presents a subtraction of LERG-OS response from TERG. With the strongest light step, the TERG responses settled to a level $34 \pm 6\%$ ($n = 5$) smaller than in LERG-OS and this difference was reached within 4 seconds from the beginning of the step response. In Figure 9B, the TERG step-flash responses of Figure 9A are normalized to their flash-response plateau amplitudes. With this normalization, the saturated TERG and LERG-OS flash responses closely correspond to each other and the time spent in complete saturation decreases systematically with increasing step-light intensity in both sets as shown in Figures 9B and 9D.

The saturation period T_{sat} was determined as the time interval from the saturating flash to the moment when the response had recovered 25% from the plateau level. The saturating flash strength used varied from 1575 to 6270 R^*rod^{-1} between experiments. The change in T_{sat} from its dark adapted value ($\Delta T = T_{sat,dark} - T_{sat,step}$) is plotted as a function of the natural logarithm of light step intensity in Figure 9F for simultaneous TERG and LERG-OS recordings. Each point represents a population-averaged value from one to four experiments. In all experiments, ΔT increased linearly with log-step intensity within a certain range of step intensities. In the linear range, ΔT was 44 ± 4 ms and 46 ± 3 ms per e-fold increase in step intensity by LERG-OS and by TERG ($n = 5$), respectively. Strong background light, which produced $85 \pm 2\%$ ($n = 5$) steady-state amplitude of the dark-adapted saturation level by LERG-OS, caused T_{sat} shortening of 189 ± 21 ms by LERG-OS and 188 ± 24 ms by TERG ($n = 5$). These results demonstrate that the relation of step-flash adaptation to stimulus strength and the maximal adaptation are similar by TERG and LERG-OS.

TERG Signal Components That Are Not Directly Related to Phototransduction

Occasionally, in our TERG recordings, we observed additional signal components merging with the known waveform, indicating that their origin is not in phototransduction. These components occurred despite of pharmacologic blocking of synapses and glial contribution, and they were more pronounced in bicarbonate than in HEPES buffered solution. As an example, Figure 10A introduces response families to 1-ms flashes in bicarbonate buffered solution where the TERG responses show prominent differences compared with the familiar shape of LERG-OS responses even when the synaptic transmission has been blocked with 20- μ M APB and 2-mM aspartate. Figure 10B illustrates the difference in the response shapes of LERG-OS and TERG. The responses were first normalized to the plateau level of saturated responses and then LERG-OS responses were subtracted from corresponding TERG responses. Subtraction revealed at least two wave components: the fast nose component and a slower component with positive polarity, whose amplitude saturated at stimulus strengths clearly below those needed to saturate normal mouse rods. To investigate further the origin of the slow positive components, we began to insert the LERG recording electrode deeper to the retina from the outer segment layer (Fig. 10C). The extra component started to merge to LERG recordings when the recording electrode intruded into the rod inner segment layer (see also Fig. 5A for nose component). The recording electrode was passed all the way to bipolar cell layer (200 μ m) but the component amplitude did not increase after the photoreceptor layer (100 μ m) but rather smoothed and started to resemble the response shape by TERG. These experiments demonstrate that besides the ERG “nose,” another component originating in rod inner segment and perhaps in the synaptic region can modulate TERG responses.

DISCUSSION

TERG detects potential changes due to the light-evoked alterations in the extracellular currents that flow radially in the retina. The technique enables long lasting and stable experiments on intact isolated retinas with excellent signal-to-noise ratio. In TERG, many individual signal components can be separated and investigated with the help of pharmacologic manipulation. When combined with the possibilities offered by gene manipulation in the production of predictive disease animal models, TERG offers an effective and versatile tool for both qualitative and quantitative examination of retinal functions. However, when TERG is used to draw conclusions about

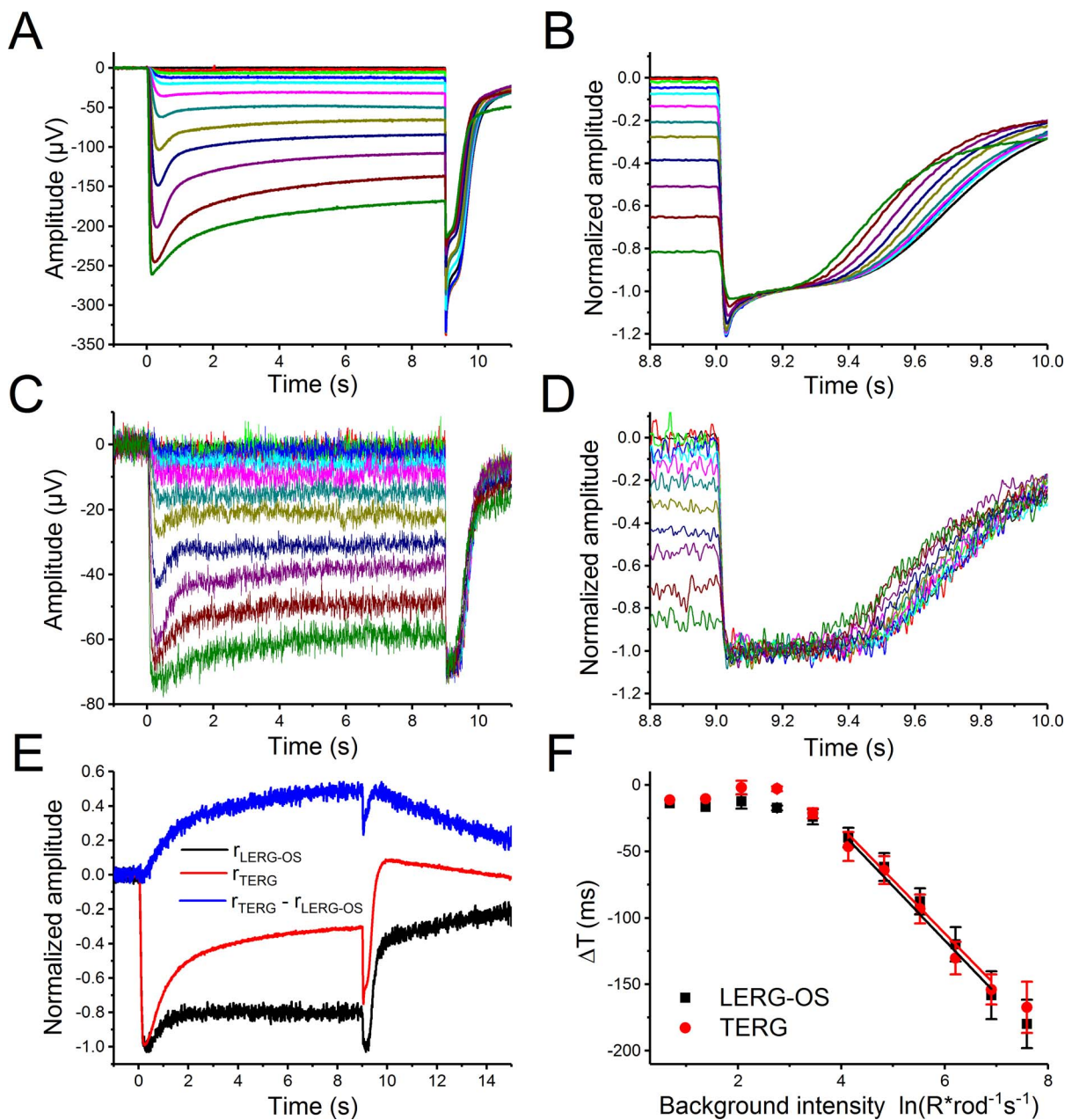


FIGURE 9. Step-flash adaptation by TERG and LERG-OS in HEPES buffered solution. Retinas were stimulated with 9-second background light steps with intensities ranging from 2 to 1980 $R^*rod^{-1}s^{-1}$ with 2-fold increments. A saturating flash ($1580 R^*rod^{-1}$) was delivered at background light turn off. Step-flash response families recorded by TERG (A) and by LERG-OS (C). (B) Saturating flash responses of panel (A) with amplitudes normalized to the flash response plateau levels. (D) LERG-OS responses normalized to their saturation levels. (E) TERG and LERG-OS step-flash responses to $1980 R^*rod^{-1}s^{-1}$ light normalized with the plateau level amplitudes of saturating flash responses in darkness and subtraction of LERG-OS response from TERG response. (F) Changes in the flash response saturation period $\Delta T = T_{sat,dark} - T_{sat,step}$ plotted against background light intensity for TERG (red) and LERG-OS (black). The error bars indicate SEMs.

the molecular mechanisms of rod phototransduction or about the actions of potential drugs on the phototransduction machinery, the potential contributions of ERG components originating in the inner segments of rods need to be considered.

TERG Responses Closely Correspond to Those Recorded by Local ERG Across Rod Outer Segments

In order to compare the TERG signal with the outer segment current signal that reflects the operation of the phototransduction machinery, we used local ERG recording (simul-

taneously with TERG) across the rod outer segment layer instead of direct recording of the current signal by suction pipette method. Several reasons favor this choice: first, it provided us the opportunity to keep the photoreceptor cells in similar conditions in both recording modalities. In suction pipette recordings, the part of the cell in the pipette is not supplied with perfusion or bicarbonate buffering. As a result, the inside of the pipette becomes a sink for carbon dioxide and the CO_2 reacting with water produces hydrogen ions in addition to bicarbonate, tending to acidify the pipette filling solution. Second, the current value recorded by the suction pipette depends on the electrical potential around the tip of

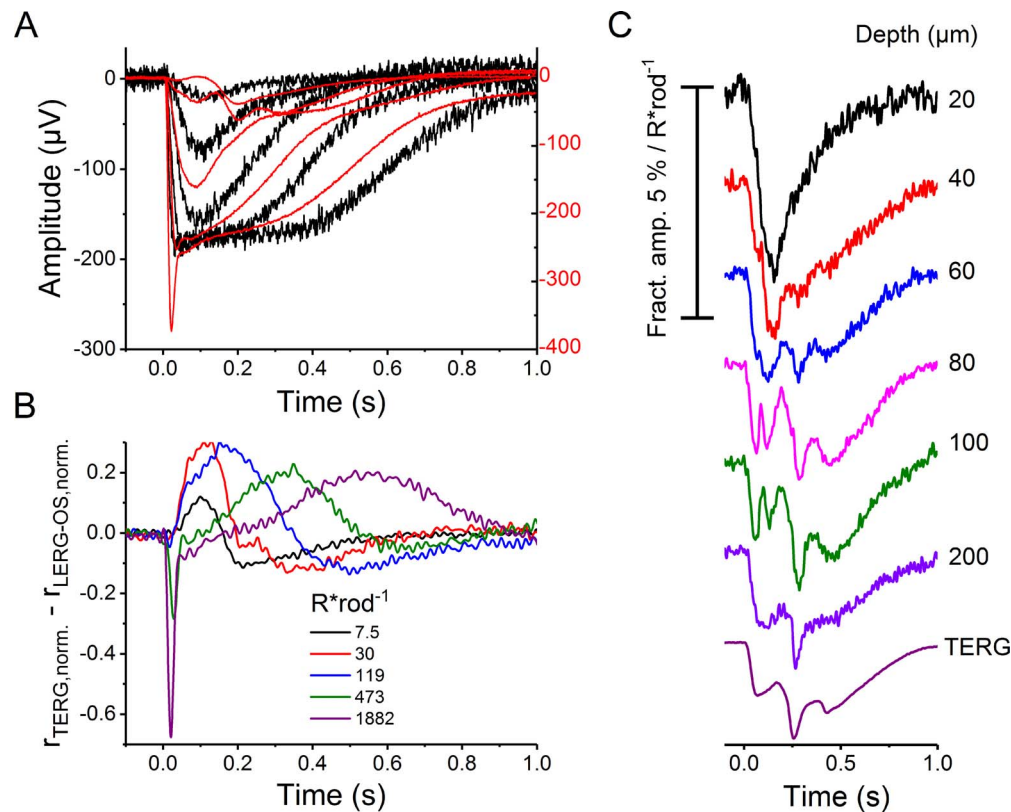


FIGURE 10. (A) A response family in bicarbonate buffered solution with 20- μM APB, 2-mM aspartate, and 50- μM BaCl_2 recorded by TERG (red) and LERG-OS (black) showing additional wave components. Stimulus strengths was varied from 7.5 to 1882 $\text{R}^*\text{rod}^{-1}$ with 4-fold increments. (B) Subtraction of normalized LERG-OS signals from normalized TERG signals to highlight the shape and kinetics of additional waves. (C) Dim flash responses (6.8 $\text{R}^*\text{rod}^{-1}$) in bicarbonate buffered solution with 20- μM APB and 50- μM BaCl_2 recorded by TERG and by LERG at various retinal depths.

the pipette. The study of Green and Kapousta-Bruneau¹⁴ suggested that the currents generated in the inner retina might affect the local potential around the photoreceptor outer segments, and thereby distort the suction pipette recordings made from flat-mounted retinas. However, our results indicate that the intraretinal components described by Green and Kapousta-Bruneau¹⁴ do not exist in LERG-OS when the proximal and distal sides of the retina are carefully electrically isolated.

The fundamental observation in this study was that the TERG flash responses correspond well with the local ERG responses recorded across the outer segment layer when the plateau in saturated TERG signal is considered as the zero level of circulating dark current. With this premise, the parameters describing photoreceptor sensitivity or light response kinetics differed not more than 40% (see Table). The major differences between the TERG and LERG-OS responses were the additional fast “nose” component and the larger signal amplitude in TERG (see Figs. 6A, 6B). The nose contains components with different kinetics and it is probably a mixture of cone contribution, a component arising from the function of the hyperpolarization activated h-channels in the photoreceptor inner segments, and a capacitive component originating mainly in the photoreceptor inner segments.^{12,19,26} With most retinas, the fractional sensitivity appeared somewhat lower in TERG than in LERG-OS. The reason for this distinction is unclear but one explanation could be local sensitivity differences in the retina. We detected local differences in rod sensitivities as well as in maximal response amplitudes and preferred the most sensitive regions in LERG-OS recordings, whereas TERG inherently records the average signal of a larger retinal area. Thus, the fractional response amplitude is expected to be

larger in LERG-OS and the maximal response amplitudes greater in LERG-PR compared with TERG. The local sensitivity differences should lead to a less steep stimulus strength–response amplitude curve in TERG compared with LERG-OS. However, our recordings showed quite the opposite (Fig. 6E). An alternative explanation for the lower sensitivity value by TERG could be that a current loop exists in the rod inner segment generating a signal of opposite polarity compared with the outer segment current. In order to produce the steeper stimulus strength–response amplitude curve observed for TERG, the extra component should have larger relative impact on dim flash than saturated responses and the maximal amplitude of that component should be much smaller than that of the normal photoresponse. Indeed, we observed such a component in a few TERG experiments but never in LERG-OS (see Fig. 10). This can, to a certain extent, explain the small differences in the parameter values from TERG and LERG-OS responses (Table). The occurrence of this component was more frequent in bicarbonate than in HEPES buffered solution. The bicarbonate buffered situation resembles more closely to the situation in vivo because bicarbonate regulates many retinal functions, including the intracellular pH,^{41,42} the guanylate cyclase activity,⁴³ and the pH of the synaptic region known to modulate the calcium currents in photoreceptors.²⁴ Nevertheless, the mechanisms responsible for generating this component remain unclear but it most likely originates in the rod inner segment and the synaptic region.

The most notable difference between responses by the ERG techniques and suction electrode recordings (SP) was the 2-fold rod sensitivity in SP. The reason for this is not completely understood but one likely and at least partial explanation is that the rod outer segments are bend in the strong perfusion in

our recording geometry, because the perfusion is oriented toward the rod longitudinal axis. Outer segment bending of approximately 50° to 60° could fully explain the sensitivity difference.

Rod Light Adaptation is Similar When Recorded by TERG and LERG-OS

The photoresponse recovery during prolonged illumination, characteristic of light adaptation in photoreceptor cells, appears quantitatively very similar in TERG and LERG-OS. Nevertheless, we found that with strong light steps the photoresponses recovered more in TERG than in LERG-OS (Figs. 7C, 9E). The difference between the TERG and LERG-OS step response recovery can be explained with an additional TERG component with a polarity opposite to the proper response and whose amplitude first grows and then settles to a constant value in a few seconds after eliciting the step light. This kind of behavior is visible also in the flash responses of the step-flash paradigm (Fig. 9). In LERG-OS recordings, the saturated flash responses at the end of the light steps settle to a common plateau corresponding to the zero outer segment current level, and the time spent in saturation (T_{sat}) decreases with increasing step intensity as previously seen in suction pipette recordings. This shortening of the saturation time indicates that the number of activated phosphodiesterases elicited by the saturating flash decreases toward stronger light-adapting steps and it is interpreted to reflect reduction of the lifetime of activated rhodopsin.^{32,39} In TERG, instead, the corresponding saturation level of the flash response is progressively diminished with increasing intensity of the light step. The quantitative agreement between the amplitude of the additional component at the end of the step response and the decrease in the saturation level of the flash response indicates a common origin for the phenomena. A recent study shows that voltage sensitive conductances in rod inner segment help rods to increase light sensitivity after strong background light.⁴⁴ The detected behavior in TERG step responses could be a consequence from inner segment current driven modulation of rod membrane voltage in order to adapt to background light. Furthermore, the scaling of the saturation amplitudes of the TERG flashes to the same level accurately reproduces the shortening of the T_{sat} that is seen in LERG-OS recordings. Overall, our results demonstrate that the step-flash paradigm of Fain et al.³² can be used with TERG provided that the “plateau” levels of the saturating flashes are scaled to coincide.

Transretinal ERG Bridges Single Cell and In Vivo Recordings

Several studies emphasize that the a- and b-waves of transretinally recorded ERG are very well comparable with those recorded corneally in vivo,^{13,15,16} suggesting that the state of the isolated retina corresponds to the state of retina in vivo. The present study takes the next step by demonstrating that pharmacologically isolated photoreceptor TERG recordings coincide well with LERG-OS (and thus with suction pipette) recordings both in dark and light adapted retinas and that TERG and LERG-OS give both qualitatively and quantitatively corresponding results with all the most common light stimulation paradigms used in phototransduction research. We conclude that the use of TERG, combined with the option for easy and accurate pharmacologic manipulation of the molecular mechanisms in retina, can satisfy the growing need for more precise, versatile, and cost-effective tools in quantitative research of retinal signaling and in preclinical drug testing.

Acknowledgements

The authors thank Jaakko Järvinen, PhD, for discussion and comments on the manuscript.

Supported by grants from The International Doctoral Programme in Biomedical Engineering and Medical Physics (Oulu, Finland), and by Oskar Öflunds Stiftelse sr (Helsinki, Finland).

Disclosure: T.T. Turunen, None; A. Koskelainen, None

References

- McCulloch DL, Marmor MF, Brigell MG, et al. ISCEV Standard for full-field clinical electroretinography (2015 update). *Doc Ophthalmol.* 2015;130:1-12.
- Rivolta C, Sharon D, DeAngelis MM, Dryja TP. Retinitis pigmentosa and allied diseases: numerous diseases, genes, and inheritance patterns. *Hum Mol Genet.* 2002;11:1219-1227.
- Ferrari S, Di Iorio E, Barbaro V, Ponzin D, Sorrentino FS, Parmeggiani F. Retinitis pigmentosa: genes and disease mechanisms. *Curr Genomics.* 2011;12:238-249.
- Vinberg F, Wang T, Molday RS, Chen J, Kefalov VJ. A new mouse model for stationary night blindness with mutant Slc24a1 explains the pathophysiology of the associated human disease. *Hum Mol Genet.* 2015;24:5915-5929.
- Zeitl C, Robson AG, Audo I. Congenital stationary night blindness: an analysis and update of genotype-phenotype correlations and pathogenic mechanisms. *Prog Retin Eye Res.* 2015;45:58-110.
- Biel M, Michalakakis S, Ludwig A, Hofmann F. Cyclic nucleotide-gated and hyperpolarization-activated channels. In: Squire LR, ed. *Encyclopedia of Neuroscience.* San Diego, CA: Elsevier Ltd; 2009:279-284.
- Remmer MH, Rastogi N, Ranka MP, Ceisler EJ. Achromatopsia: a review. *Curr Opin Ophthalmol.* 2015;26:333-340.
- Hamel CP. Cone rod dystrophies. *Orphanet J Rare Dis.* 2007; 2:7.
- Vinberg F, Turunen TT, Heikkinen H, Pitkänen M, Koskelainen A. A novel Ca²⁺-feedback mechanism extends the operating range of mammalian rods to brighter light. *J Gen Physiol.* 2015;146:307-321.
- Nymark S, Heikkinen H, Haldin C, Donner K, Koskelainen A. Light responses and light adaptation in rat retinal rods at different temperatures. *J Physiol.* 2005;567(Pt 3):923-938.
- Donner K, Hemila S, Koskelainen A. Temperature-dependence of rod photoresponses from the aspartate-treated retina of the frog (*Rana temporaria*). *Acta Physiol Scand.* 1988;134: 535-541.
- Vinberg F, Strandman S, Koskelainen A. Origin of the fast negative ERG component from isolated aspartate-treated mouse retina. *J Vis.* 2009;9:9.1-9.17.
- Vinberg F, Kolesnikov AV, Kefalov VJ. Ex vivo ERG analysis of photoreceptors using an in vivo ERG system. *Vision Res.* 2014;101:108-117.
- Green DG, Kapousta-Bruneau NV. A dissection of the electroretinogram from the isolated rat retina with micro-electrodes and drugs. *Vis Neurosci.* 1999;16:727-741.
- Green DG, Kapousta-Bruneau NV. Electrophysiological properties of a new isolated rat retina preparation. *Vision Res.* 1999;39:2165-2177.
- Heikkinen H, Vinberg F, Pitkänen M, Kommonen B, Koskelainen A. Flash responses of mouse rod photoreceptors in the isolated retina and corneal electroretinogram: comparison of gain and kinetics. *Invest Ophthalmol Vis Sci.* 2012;53:5653-5664.
- Arden GB. Voltage gradients across the receptor layer of the isolated rat retina. *J Physiol.* 1976;256:333-360.1.

18. Reiser MA, Williams TP, Pugh EN. The effect of light history on the aspartate-isolated fast-PIII responses of the albino rat retina. *Invest Ophthalmol Vis Sci.* 1996;37:221-229.
19. Robson JG, Frishman LJ. The rod-driven a-wave of the dark-adapted mammalian electroretinogram. *Prog Retin Eye Res.* 2014;39:1-22.
20. Baylor DA, Lamb TD, Yau KW. The membrane current of single rod outer segments. *J Physiol.* 1979;288:589-611.
21. Hagins WA, Penn RD, Yoshikami S. Dark current and photocurrent in retinal rods. *Biophys J.* 1970;10:380-412.
22. Bolnick DA, Walter AE, Sillman AJ. Barium suppresses slow PIII in perfused bullfrog retina. *Vision Res.* 1979;19:1117-1119.
23. Cadetti L, Thoreson WB. Feedback effects of horizontal cell membrane potential on cone calcium currents studied with simultaneous recordings. *J Neurophysiol.* 2006;95:1992-1995.
24. Warren TJ, Van Hook MJ, Supuran CT, Thoreson WB. Sources of protons and a role for bicarbonate in inhibitory feedback from horizontal cells to cones in *Ambystoma tigrinum* retina. *J Physiol.* 2016;594:6661-6667.
25. Govardovskii VI, Fyhrquist N, Reuter T, Kuzmin DG, Donner K. In search of the visual pigment template. *Vis Neurosci.* 2000;17:509-528.
26. Heikkinen H, Nymark S, Koskelainen A. Mouse cone photoresponses obtained with electroretinogram from the isolated retina. *Vision Res.* 2008;48:264-272.
27. Lamb TD, Pugh EN. A quantitative account of the activation steps involved in phototransduction in amphibian photoreceptors. *J Physiol.* 1992;449:719-758.
28. Gross OP, Pugh EN, Burns ME. Spatiotemporal cGMP dynamics in living mouse rods. *Biophys J.* 2012;102:1775-1784.
29. Ortin-Martinez A, Nadal-Nicolas FM, Jimenez-Lopez M, et al. Number and distribution of mouse retinal cone photoreceptors: differences between an albino (Swiss) and a pigmented (C57/BL6) strain. *PLoS One.* 2014;9:e102392.
30. Azevedo AW, Rieke F. Experimental protocols alter phototransduction: the implications for retinal processing at visual threshold. *J Neurosci.* 2011;31:3670-3682.
31. Vinberg F, Kefalov V. Simultaneous ex vivo functional testing of two retinas by in vivo electroretinogram system. *J Vis Exp.* 2015;99:e52855.
32. Fain GL, Lamb TD, Matthews HR, Murphy RL. Cytoplasmic calcium as the messenger for light adaptation in salamander rods. *J Physiol.* 1989;416:215-243.
33. Pepperberg DR, Cornwall MC, Kahlert M, et al. Light-dependent delay in the falling phase of the retinal rod photoresponse. *Vis Neurosci.* 1992;8:9-18.
34. Sarfare S, McKeown AS, Messinger J, et al. Overexpression of rod photoreceptor glutamic acid rich protein 2 (GARP2) increases gain and slows recovery in mouse retina. *Cell Commun Signal.* 2014;12:67.
35. Nikonov SS, Kholodenko R, Lem J, Pugh EN. Physiological features of the S- and M-cone photoreceptors of wild-type mice from single-cell recordings. *J Gen Physiol.* 2006;127:359-374.
36. Chen C-K, Woodruff ML, Chen FS, Shim H, Cilluffo MC, Fain GL. Replacing the rod with the cone transducin subunit decreases sensitivity and accelerates response decay. *J Physiol.* 2010;588(Pt 17):3231-3241.
37. Woodruff ML, Rajala A, Fain GL, Rajala RVS. Modulation of mouse rod photoreceptor responses by Grb14 protein. *J Biol Chem.* 2014;289:358-364.
38. Matthews HR. Static and dynamic actions of cytoplasmic Ca²⁺ in the adaptation of responses to saturating flashes in salamander rods. *J Physiol.* 1996;490(Pt 1):1-15.
39. Nikonov S, Lamb TD, Pugh EN. The role of steady phosphodiesterase activity in the kinetics and sensitivity of the light-adapted salamander rod photoresponse. *J Gen Physiol.* 2000;116:795-824.
40. Makino CL, Dodd RL, Chen J, et al. Recoverin regulates light-dependent phosphodiesterase activity in retinal rods. *J Gen Physiol.* 2004;123:729-741.
41. Donner K, Hemila S, Kalamkarov G, Koskelainen A, Shevchenko T. Rod phototransduction modulated by bicarbonate in the frog retina: roles of carbonic anhydrase and bicarbonate exchange. *J Physiol.* 1990;426:297-316.
42. Saarikoski J, Ruusuvaara E, Koskelainen A, Donner K. Regulation of intracellular pH in salamander retinal rods. *J Physiol.* 1997;498(Pt 1):61-72.
43. Duda T, Wen X-HH, Isayama T, Sharma RK, Makino CL. Bicarbonate modulates photoreceptor guanylate cyclase (ROS-GC) catalytic activity. *J Biol Chem.* 2015;290:11052-11060.
44. Pahlberg J, Frederiksen R, Pollock GE, Miyagishima KJ, Sampath AP, Cornwall MC. Voltage-sensitive conductances increase the sensitivity of rod photoresponses following pigment bleaching. *J Physiol.* 2017;595:3459-3469.
45. Sakurai K, Young JE, Kefalov VJ, Khani SC. Variation in rhodopsin kinase expression alters the dim flash response shut off and the light adaptation in rod photoreceptors. *Invest Ophthalmol Vis Sci.* 2011;52:6793-6800.
46. Gross OP, Pugh EN, Burns ME. Calcium feedback to cGMP synthesis strongly attenuates single-photon responses driven by long rhodopsin lifetimes. *Neuron.* 2012;76:370-382.